The effect of rocking excitation on the dynamic behaviour of a Nuclear Power Plant reactor building with base isolation

M. Domaneschi, L. Martinelli, F. Perotti
Department of Structural Engineering, Politecnico di Milano, Milano, Italy

SUMMARY:

Past research has shown that for seismically isolated Nuclear Power Plants (NPPs) rocking has little effects on the peak bearing deformation or axial forces. Recently however, a new class of special buildings has been considered for seismic isolation, namely Generation 3+ and 4 Nuclear Power Plant reactor buildings. The safety issues related to NPPs suggest an assessment of previous results also for these new structures.
Since rocking motion can be triggered by earthquake surface waves, this work compares the effects of two different description for earthquake motions through coherency functions on a simplified model of the NPP reactor building set on laminated metal-rubber bearings. The model is subject to synthetic generated accelerograms which satisfy a modified Kanai-Tajimi power spectral density. The laminated metal-rubber bearings are modelled with a non-linear cyclic force-displacement law for the horizontal displacements and are vertically linearly elastic.

Keywords: NPP reactor building; seismic isolation; rocking; earthquake rotational component

1. INTRODUCTION

While rocking has been considered in the past for building seismically isolated by vertical steel springs, the high axial stiffness of laminated rubber-metal bearing has allowed to consider this as a secondary problem whenever this (more common) isolation system is selected for buildings. For the latter isolation system the motion of the isolated part is traditionally assumed to be quasi-horizontal, with only minor rotation components (Rivin, 2003) and rocking has been found to have little effects on the peak bearing deformation or axial forces (Ryan and Chopra, 2006). In (Politopoulos, 2009) it is shown that, in the case of classical horizontal isolation, rocking input may amplify significantly the response of the lower non-isolated modes.
Recently however, a new class of special structures has been considered for seismic isolation, namely the reactor buildings of Nuclear Power Plants pertaining to the so-called generation 3+ and 4. The safety issues related to NPPs, the compact shape and the relevant mass of this type of buildings suggest however further investigations with respect to this phenomena, also in view of the limits shown by existing models for isolation bearings.
Since rocking motion can be triggered not only by the isolation system kinematics but also by earthquake surface waves, this work considers (a) the choice of two different coherency models for earthquake motions, with particular attentions to those suitable to describe short distance variations; (b) a simplified model of the Generation 3+ IRIS (International Reactor Innovative and Secure - Carelli et al., 2004) NPP reactor building set on laminated metal-rubber bearings subject to synthetic generated accelerograms; (c) a non-linear model for the laminated metal-rubber bearings, which follows a non-linear cyclic force-displacement law for the horizontal displacements while are linearly elastic for the vertical ones.
A recent literature model is used that relates the rotational accelerations to vertical accelerations due to the earthquake. This is adopted for generating the rotational ground accelerations.

The horizontal and the vertical components of the ground acceleration satisfy one of the selected coherency functions and a modified Kanai-Tajimi power spectral density that has been tailored so that the acceleration average response spectrum is compatible with a code prescribed one (here that in EN 1998).

2. THE IRIS REACTOR BUILDING

The IRIS (International Reactor Innovative and Secure) is a small (335 MWe) modular integral Nuclear Power Plant (NPP) object of a research program developed by an international team coordinated by Westinghouse and involving 24 organizations from 10 countries around the World, spanning from industries to universities and from utilities to national laboratories. The IRIS reactor vessel has been devised not only for housing the nuclear fuel and control rods, but also all the major reactor coolant system components. The IRIS integral vessel is larger than a traditional Pressurized Water Reactors (PWR) pressure vessel, but the size of the IRIS containment is a fraction of corresponding loop reactors, resulting in a significant reduction in the overall size of the reactor plant (Carelli et al., 2004).
The safety-by-design ^{TM} approach is adopted for the IRIS design resulted in the elimination by design of some of the main accident scenarios characterizing Pressurized Water Reactors (PWR) and in the limitation of either consequences of the remaining classical accident initiators. As a result of such strategy the Core Damage Frequency (CDF) from at-power internal initiating events is reduced to the 10^{-8}/ry order of magnitude. Then, CDF from external events, and the seismic one in particular, turns out to be the most significant contributor (De Grandis et al., 2009). Hence, in the next future the adoption of seismic isolation systems in the NPPs design is likely to become a widespread measure due to a foreseen better performance of the isolated structure when compared to traditional buildings, and thanks to the ability to maintain functionality after the event (Forni et al., 2010).

3. IRIS NUMERICAL MODEL AND SEISMIC ISOLATION

In a tentative design of the Nuclear Steam Supply System (NSSS) the introduction of an isolation system was considered (see Figure 1a); the system consists in High Damping Rubber Bearings (HDRB) installed between the foundation slab and the base (Figure 1b). The HDRB devices are made of alternated rubber layers and steel plates, bonded through vulcanization. Damping factor ranges from 10% to 20%, while shear modulus (G) at 100% shear deformation lies in the 0.8-1.4 MPa range.
Steel plates give a high vertical stiffness to the isolator, though allowing large horizontal deformations. Therefore, the isolated building has low natural frequencies for motions lying in the horizontal plane, typically in the range 0.5 - 0.7 Hz, where the spectrum of ground motion has generally quite low energy. In such vibration modes the isolated building moves like a rigid body (see also Forni et al., 2010) over the isolators, which are strained in shear (continuously carrying the dead load). The absolute acceleration of the building can be much smaller than the PGA, with no amplification at higher floors. This is obtained at the price of large relative displacements between the building and the adjacent ground; this can be a problem for the design of the expansion joints and the connections with non isolated buildings of all the pipelines and service networks. The design of the isolation system, therefore, must reach a reasonable compromise between limitation of absolute accelerations and relative displacements. For the case of the IRIS NSSS, having a fixed-base first natural frequency of 5.91 Hz (on firm ground) and natural frequencies around 9 Hz for the vessel local motion, this led to a 0.7 Hz isolation frequency, i.e. to a value which can be seen as an upper limit for the parameter. If some equipment component (e.g., some wide span pipeline) has a lower natural frequency a local specific measure (stiffening or energy dissipation device) must be adopted.
The choice of 0.7 Hz as isolation frequency limits the relative displacement between the isolated building and the ground to 10 cm at the Safe Shutdown Earthquake (SSE) level, which is advantageous both for the performance of the isolators in beyond design conditions and for the design of steam lines connecting the NSSS building with the turbine units.
To compute the fragility of the IRIS isolation system a first 3-DOFS plane model has been adopted for

the reactor building (Perotti et al., 2011), under the hypothesis that the isolated superstructure behaves like a rigid body; soil-structure interaction has been neglected. The behaviour of isolators under horizontal and vertical loading has been regarded as independent; it is assumed that isolators behave as linear elastic under vertical loading, showing the same stiffness in tension and compression. Their non linear behavior under horizontal loading has been modeled according to the uni-directional models described in the next section.

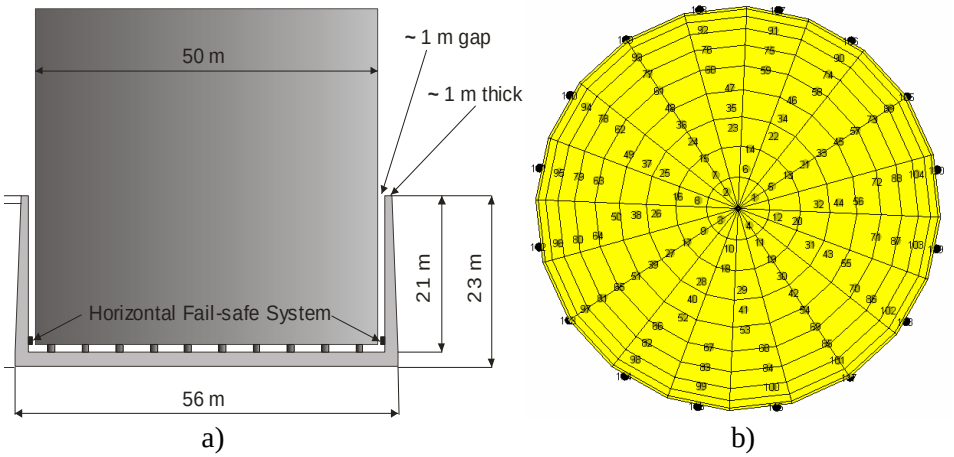

Figure 3.1. IRIS NSSS building (a); isolators layout (b)

3.1. Numerical model of the HDRBs

HDRBs are modeled according to the unidirectional approach in Abe et al. (2004) since it allows to reproduce analytically some important aspects of the experimental behavior of laminated rubber bearings. The restoring force is the sum of three contributions (Fig. 3.2a): an elastic non-linear spring (F_1), an elastic-plastic spring (F_2) and a hardening spring (F_3).

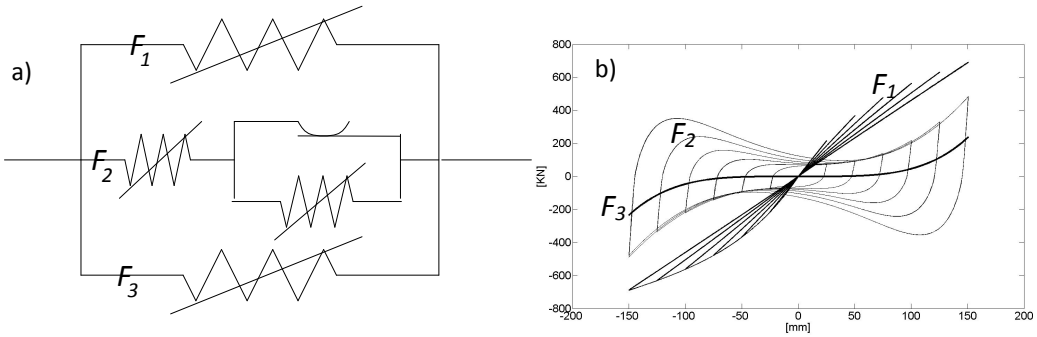

Figure 3.2. Scheme of the HDRB model (Abe et al., 2004) (a); F_1,F_2,F_3 components under cyclic loading (b)

The force-displacement relation for non-linear spring F_1 is:

$$F_1 = K_1\left\{\beta + (1-\beta)\exp\left(-\frac{U_{\max}}{\alpha}\right)\right\}U + a\left[1-\exp(-b|U|)\right]\mathrm{sgn}(U) \tag{3.1}$$

where U is the relative displacement and K_1, α and β are parameters. In Equation (3.1), the first term reproduces the force linear evolution, while the second one the non-linear behaviour. Figure 3.2b depicts the contribution of F_1, for a cyclic experimental test on a reference specimen, as force vs. displacement up to values of displacement equal to 300% of the rubber height. The stiffness degradation during the variable cycle amplitude is also highlighted in this Figure.
The hysteretic contribution of F_2 is described through the differential equation:

$$\dot{F}_2 = \frac{Y_t}{U_t}\left\{\dot{U} - \left|\dot{U}\right|\left|\frac{F_2}{Y_t}\right|^n \operatorname{sgn}\left(\frac{F_2}{Y_t}\right)\right\} \tag{3.2}$$

where the values of Y_t and U_t are defined as

$$Y_t = Y_0\left(1 + \left|\frac{U}{U_H}\right|^p\right) \quad ; \quad U_t = U_0\left(1 + \frac{U_{\max}}{U_S}\right) \tag{3.3}$$

and Y_0 is the initial yielding force, U_0 the initial yielding displacement, U_H the displacement where hardening starts, U_S a parameter for controlling the degradation of the elastic stiffness, U_{max} the maximum displacement experienced during the previous loading history, p a parameter governing the shape of the hardening branch.
The F_3 non-linear spring is introduced for capturing the increment of the tangential stiffness experienced by the HDRBs devices at very high strain levels:

$$F_3 = K_2\left|\frac{U}{U_H}\right|^r U \tag{3.4}$$

where r is the parameter to prescribe the shape of the hardening curve, K_2 the proportional constant which describes the contribution of the hardening spring with respect to the other springs.

3.2. 3-DOFs model of the IRIS NPP reactor building

The reactor building is modelled as a cylindrical rigid body supported by a bed of HDRBs in an axisymmetric configuration (see Figure 3.1b). The passive control system is characterized by shear deformability and the Lagrangian coordinates for the rigid body are horizontal translation (q_1), vertical translation (q_2) and rotation (q_3) of the centre of mass. The centroid G of the main building of the IRIS NPP is located at a height of 18.65m from the plane of the isolation system.
Taking into consideration the horizontal hysteretic reaction force computed by the Abe et al. (2004) unidirectional model, the following system of equations of motion is derived:

$$m\ddot{q}_1 + nF_f = -ma_o + mz_G a_{rot} \tag{3.5}$$

$$m\ddot{q}_2 + c_v n\dot{q}_2 + c_v\sum_{i=1}^{n}(x_i - x_G)\dot{q}_3 + k_v n q_2 + k_v\sum_{i=1}^{n}(x_i - x_G)q_3 = 0 \tag{3.6}$$

$$I_G\ddot{q}_3 + nz_G F_f + c_v\sum_{i=1}^{n}(x_i - x_G)\dot{q}_2 + c_v\sum_{i=1}^{n}(x_i - x_G)^2\dot{q}_3 + $$
$$+ k_v\sum_{i=1}^{n}(x_i - x_G)q_2 + k_v\sum_{i=1}^{n}(x_i - x_G)^2 q_3 = -I_G a_{rot} \tag{3.7}$$

Where n is the number of the adopted HDRBs, x_G and z_G the centroidal coordinates from the base isolation system, m is the concentrated mass of the NPP, I_G its inertia moment about a centroidal axis, a_{rot} the ground rotational acceleration due to the earthquake, a_0 the ground translational acceleration assumed respectively in the same direction of q_1 and q_3. F_f is the hysteretic control force relative to each passive base isolation device:

$$F_f = F_1 + F_2 + F_3 \tag{3.8}$$

In Equations 3.5 is possible to recognize the amplification due to the rotational response term on the hysteretic control force F_f which is amplified by the z_G coordinate of the extrados of the isolation plane. Further details on the modelling can be found in Perotti et al. (2011).

3.3. Parameters of the isolation devices

Experimental tests of the behavior of the adopted HDRB devices under imposed cyclic relative displacements and constant axial force have been carried on ½ scaled HDRB seismic isolator prototypes, due to the very large dimensions of the HDRB elastomeric devices specifically designed for the IRIS reactor building. The tested prototypes have the following characteristics: isolator external diameter = 500mm, steel reinforcing plate diameter = 480mm, thickness of internal steel plates = 2mm, number of elastomeric layers = 10, thickness of an individual elastomeric layer = 5mm, total elastomeric thickness = 50mm, first shape factor = 24.0, second shape factor = 9.60, full isolator height = 128mm, nominal dynamic shear modulus = 1.4 MPa, hardness = 75 Shore A3, equivalent viscous damping coefficient= 10/15 %. Vertical compression and shear tests up to collapse have been performed; in the latter, maximum shear deformation has exceeded 300%. Details on the behaviour at the ultimate limit state of the seismic device can be found in ENEA 2010.
Satisfactory tests have been performed on several isolator prototypes by adopting the model proposed by Abe et al. (2004 - see Section 3.1). The model capabilities can be appreciated in Figure 3.3 where. its results (thick line) are compared to the experimental behavior (thin line) for a cyclic shear tests in quasi-static condition (0.005mm/s), showing an extremely good accuracy up to an average shear deformation of about 300%.

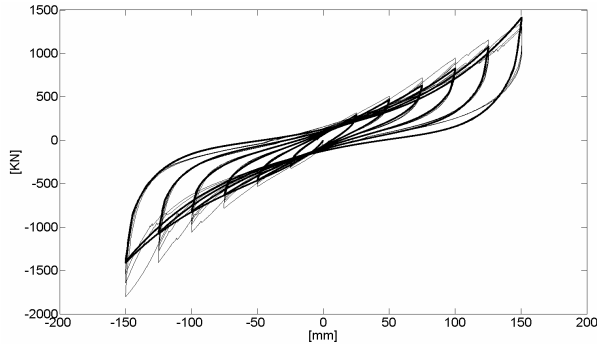

Figure 3.3. Comparison of experimental (thin line) and numerical (thick line) experimental behaviour for a cyclic test: 50%, 100%, 150%, 200%, 250%, 300% shear deformations with constant axial force (2000kN).

The Abe et al. (2004) model parameters were finally converted from the ½ scale to the full scale for simulating the isolators into the dynamic analyses of the NPP.

4. NUMERICAL GENERATION OF TRANSLATIONAL AND ROTATIONAL EARTHQUAKE ACCELERATIONS

Several sets of uncorrelated horizontal and rotational accelerogram components have been numerically generated to study the combined effects on the NPP simplified model with non-linear hysteretic isolation devices described in Section 3.
Rotational components of the accelerogram were derived from the vertical acceleration components according to the model in Castellani et al. (2012).
Horizontal and vertical acceleration time histories were generated with the procedure described in Martinelli et al. (2011).

4.1 Generation of the vertical and horizontal components

A set of horizontal and vertical acceleration time histories, on average compatible with the EN 1998

horizontal and vertical response spectra for a soil type C, were generated with the procedure described in Martinelli et al. (2011). The generation procedure is based on having previously identified the optimal parameters of the Kanai-Tajimi Power Spectral Density (MKT PSD), as modified by Clough and Penzien 1975, so that the corresponding acceleration response spectrum RS_a minimize the distance with a target one. Here the spectrum in EN 1998 for a far field event (Type 1) and a soil class "C".
The MKT PSD (Clough and Penzien 1975) can be viewed as the effect of a filter, representing the soil, on a white noise process of intensity S_0 which represents, in turn, the motion of the bedrock:

$$S_{MKT} = S_0 \frac{\omega_1^4 + 4\xi_1^2\omega_1^2\omega^2}{\left(\omega_1^2 - \omega^2\right)^2 + 4\xi_1^2\omega_1^2\omega^2} \frac{\omega^4}{\left(\omega_2^2 - \omega^2\right)^2 + 4\xi_2^2\omega_2^2\omega^2} \tag{4.1}$$

ω_1 and ξ_1 are the parameters of the Kanai-Tajimi filter representing the soil natural frequency and damping ratio, respectively, while ω_2 and ξ_2 are the parameters of an additional high-pass filter introduced by Clough and Penzien to guarantee that displacements possess finite power.
Once the parameters of the MKT-PSD are known, the acceleration time histories are generated allowing the implementation in Monti et al. (1996) of the classical wave superposition technique by Shinozuka 1972.
The parameters of the MKT PSD corresponding to the EN 1998—1 elastic response spectra were first found in Martinelli et al. (2001); those to match the EN 1998—1 horizontal elastic design spectrum S_e are $S_0 = 1.953\text{x}10^{-3}$ $m^2s^{-4}Hz^{-1}$, $\omega_1 = 12.02$ rad/s, $\zeta_1 = 0.6926$, $\omega_2 = 0.3180$ rad/s, $\zeta_2 = 3.971$. While those required to match the vertical elastic design one S_{ve} are $S_0 = 3.382\text{x}10^{-4}$ $m^2s^{-4}Hz^{-1}$, $\omega_1 = 53.95$ rad/s, $\zeta_1 = 0.6338$, $\omega_2 = 3.50$ rad/s, $\zeta_2 = 1.22$.
In Figure 4.1 the theoretical average pseudo-acceleration spectra of the ground motion are compared with those of EN 1998 for the horizontal and vertical component, respectively.

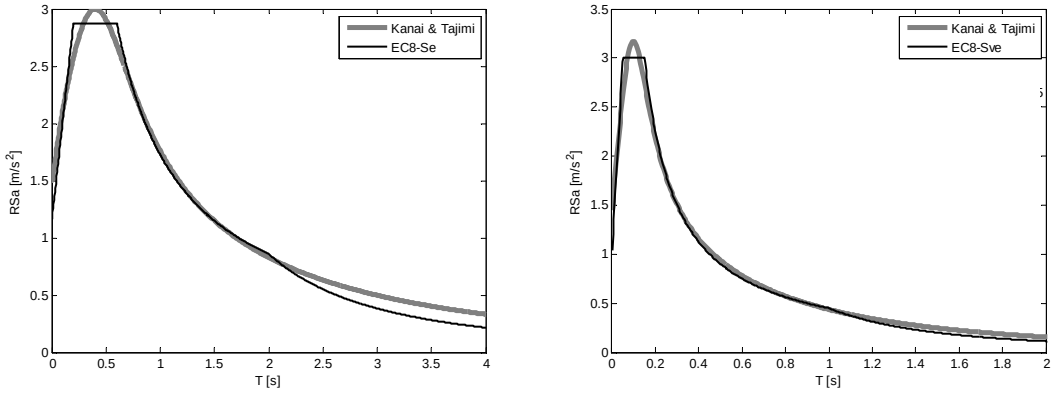

Figure 4.1. Comparison EN 1998-1 Type1 soil Type C horizontal response spectrum (a). EN 1998-1 Type1 & Type 2 response spectrum for the vertical component, all soil types (b).

4.2 Generation of the rotational component

In the model by Castellani et al. (2012) the PSD of the rotational acceleration $S_\phi(\omega,d)$ is related to that of the vertical acceleration $S_v(\omega,d)$ at two points, at a relative distance d, in the following way:

$$S_\phi(\omega,d) = \left[\frac{2S_v(\omega,d)}{d^2}\right]\left(1 - Re[\gamma_v(\omega,d)]\right) \tag{4.2}$$

Where ω is the circular frequency, $Re[\gamma_v(\omega,d)]$ is the real part of the coherency function γ_v. The distance d is the distance over which the rotation is computed as instantaneous difference between the vertical positions and it assumes the meaning of a characteristic distance for the foundation system.
Equation 4.1 implies the use of a coherency function. Two different such functions have been selected in this study, the well known coherency function by Luco and Wong 1986 and a more recent one by

Abrahamson et al. (1991), to match the one used in the work by Castellani et al. (2012). The coherency function by Luco and Wong 1986, disregarding local effects, results:

$$\gamma(\xi,\omega) = e^{-\left(\frac{\alpha\omega\xi}{v_s}\right)^2} e^{i\frac{\omega\xi_L}{v_{app}}} \tag{4.3}$$

In Equation 4.3 the modulus decays exponentially with the horizontal distance ξ between the stations, with the circular frequency ω, and inversely with the mechanical properties of the ground condensed by the ratio v_s/α. The phase depends linearly on ω, on the relative distance ξ_L and on the inverse of the apparent velocity at the surface, v_{app}, of the seismic waves. In the generation process, the phase given by the imaginary part in (4.3) leads to a time delay that can be added at a later stage.

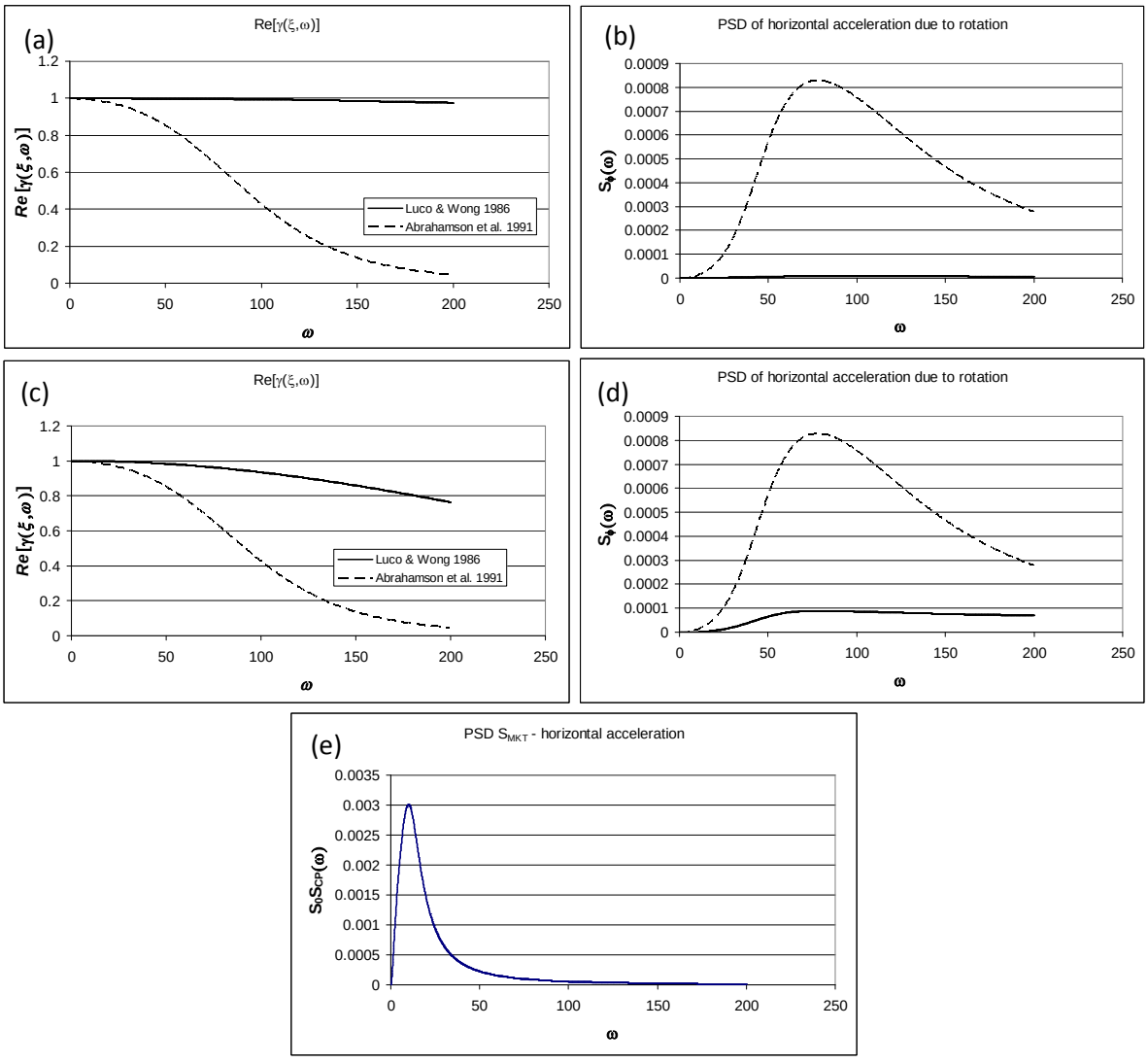

Figure 4.2. Comparison of PSD of the horizontal acceleration due to the rotational earthquake acceleration component.(a) real part of the coherency functions for $\alpha = 0.2$. (b) horizontal accelerations due to rotations for $\alpha = 0.2$. (c) real part of the coherency functions for $\alpha = 0.625$. (d) horizontal accelerations due to rotations for $\alpha = 0.65$. (e) PSD for the horizontal component of the acceleration.

The Abrahamson et al. (1991) coherency function is:

$$\tanh^{-1}|\gamma(f,\xi)| = (2.54 - 0.012\xi)\left[\exp\{(-0.115 - 0.00084\xi)f\} + \frac{f^{-0.878}}{3}\right] + 0.35 \quad (4.4)$$

where f is the frequency in Hz and ξ is the distance between the stations, in meters.
In the generation of the rotational component of the earthquake for the Luco and Wong coherency function the shear waves velocity has been assumed as v_s = 2500 ms^{-1}, two values of the incoherence factor have been considered: α = 0.20 and α = 0.625. The former leads to a rather high correlation, the last is often assumed as a reference value for moderately correlated cases. Finally, for both coherency functions the distance over which the rotational component is computed is $d = x$ = 10 m.
In Figure 4.2 a comparison is shown between the PSD of the horizontal acceleration at the reactor building centroid G (18.65 m above the isolation plane) due to the rotational earthquake acceleration component descending from the two coherency function. In Figure 4.2e the PSD for the horizontal component of the acceleration is shown as well for comparison purposes. For the Luco & Wong 1986 function two incoherency factor (α = 0.2 and α = 0.65) have been considered along with v_s = 2500 m/s. As it can be appreciated, the choice of the coherency function is of paramount importance for the rotational acceleration component, leading to contributions that range from negligible to values of the same order of that of the horizontal components of the earthquake acceleration.

Table 5.1. Average extreme values over ten realization due to horizontal and rotational acceleration components.

Case	Acceleration component	Relative displacement [m]	Absolute acceleration [m/s^2]	Vertical force [kN]
PGA = 0.35g	Rotational	0.0038	0.0939	8356.90
	Horizontal	0.147	1.9991	10272.00
	Both	0.1471	2.0116	11196.00
PGA = 0.70 g	Rotational	0.0106	0.2108	14785.00
	Horizontal	0.2425	5.6945	16970.00
	Both	0.2429	5.7362	18427.00

Table 5.2. Standard deviation over ten realizations.

Case	Acceleration component	Relative displacement [m]	Absolute acceleration [m/s^2]	Vertical force [kN]
PGA = 0.35g	Rotational	0.0012	0.0252	228.60
	Horizontal	0.0334	0.7051	1085.40
	Both	0.0349	0.7412	1217.20
PGA = 0.70 g	Rotational	0.0021	0.0312	732.39
	Horizontal	0.0367	2.1485	4157.50
	Both	0.0376	2.2361	4452.30

5. NUMERICAL ANALYSES

With the procedure briefly summarized in Section 4, two uncorrelated sets of acceleration records were generated: the first is representative of the horizontal component of an earthquake that has response spectrum compatible with the one in EN 1998—1 (S_e) for the horizontal component for soil Type “C” and spectrum of Type “1”. The second, representative of the vertical component, has been computed at two station at a distance d = 10m for both the coherency functions of Luco & Wong 1986 and of Abrahamson et al. (1991). From these accelerations the rotational component has been computed. Horizontal and rotational acceleration component records have been subsequently paired and applied on the 3-DOFs model of the Generation 3+ NPP described in Section 3, considering the non-linear model of the HDRBs by Abe et al. (2004), for two intensities of the seismic action, namely for a Peak Ground Acceleration (PGA) or 0.35 g and 0.70 g. In Table 5.1 some representative results are reported in terms of averages of extreme values of the absolute acceleration at the NPP centroid, of the relative displacement between the ends of the isolator devices and of the axial force in the farthest device. Relative displacements and axial forces are useful for sizing/checking the HDRBs, while absolute acceleration are of interest for design/checking the equipment inside the reactor building. Results pertains only the coherency function by Abrahamson et al. 1991, due to the negligible effects

expected from the PSD related to the Luco & Wong 1986 coherency function. In Table 5.2 the standard deviations for the same quantities are reported.
The results in Table 5.1 and in Section 4.2 confirm for the analysed IRIS Generation 3+ NPP building that the rocking component of the acceleration has a small effect on the relative displacements and absolute accelerations, while it induces roughly a 10/15% variation in the values of the axial forces. The computed effects from the non-linear model fall a little short of those than that can be calculated by adoption of a superposition rule like the SRSS (Square Root of Sum of Squares). Justified in this case due to the large difference between the modal period of the translational and rotational mode of the NPP 3DOFs model. Figures 5.1 and 5.2 depict representative isolator cycles and the evolution in time of the axial force, respectively, both for a PGA of 0.35 g and 0.70 g. For the latter case a large effect of the rotational ground acceleration on axial forces in the devices is highlighted, being the outermost device even in tension. This couples with the fact that the devices reach the hardening part of their characteristics.
The extreme compressive axial force is of concern since it reaches 18000 kN on average and 23000 kN for the average plus one standard deviation. Such an high value would have required adoption of a larger number of devices or larger diameters. This increase can have, however, consequences on the period of the horizontal mode if different rubber compounds are not adopted.

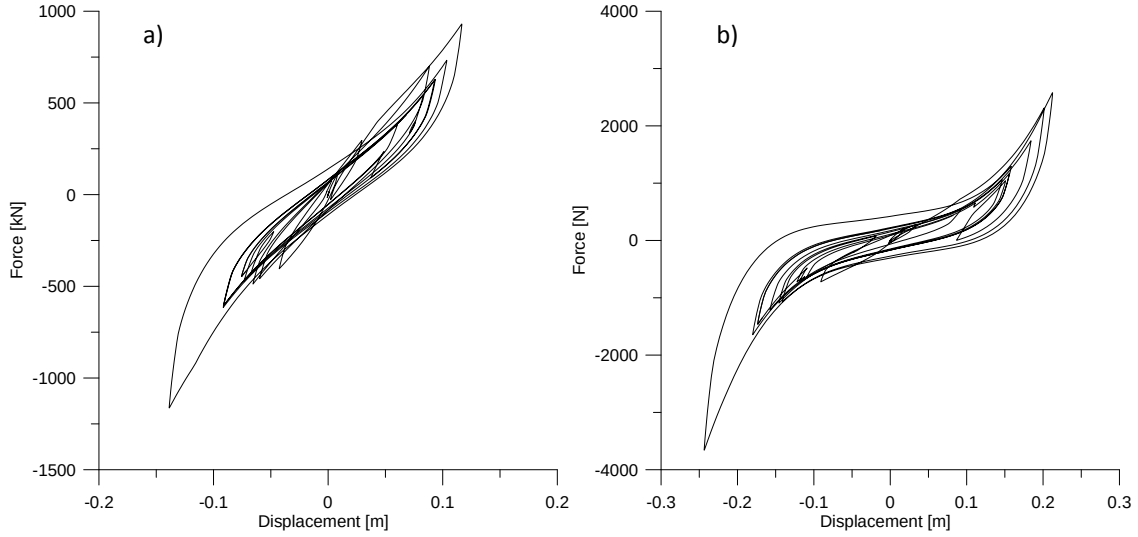

Figure 5.1. Hysteresis cycles for an isolator: (a) 0.35g; (b) 0.7g.

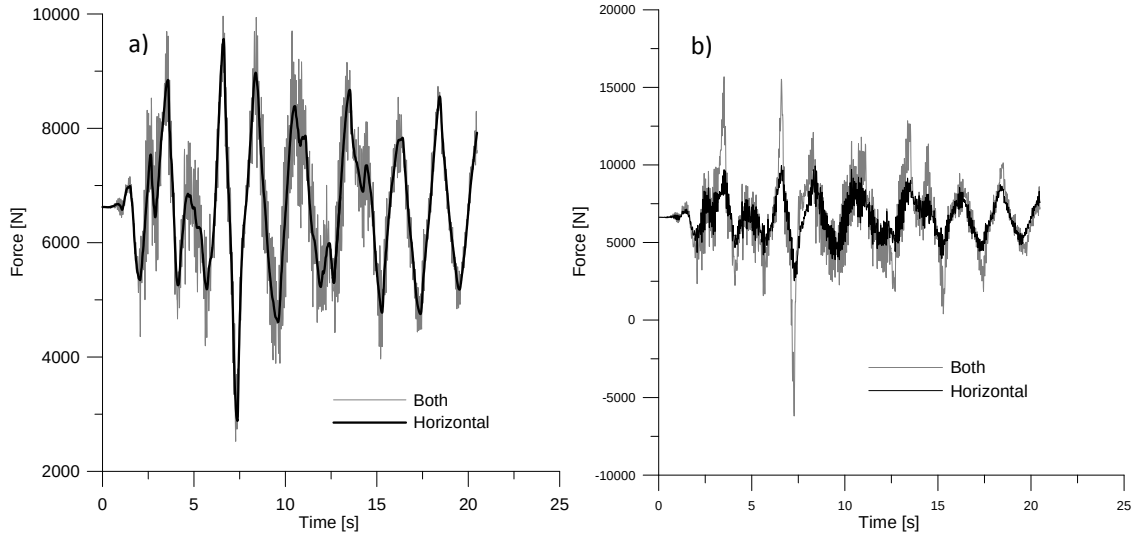

Figure 5.2. Vertical forces in the outermost isolator: (a) 0.35g; (b) 0.7g. Grey line = both ground horizontal and rotation acceleration components; black line = ground horizontal acceleration component only.

6. CONCLUSIONS

Numerical time-histories analyses carried out on a 3-DOFs model of a seismic isolated Generation 3+ NPP, considering a non-linear hysteretic model of the isolation devices, point out that using literature models for the stochastic description of the spatial variability of the seismic induced ground motion leads to a small contribution of the ground rotational acceleration to structural response, both in terms of absolute accelerations or displacements. An appreciable effect is however detected on the axial forces in the isolation devices. This is partially in contrast with the findings of past research for seismically isolated NPPs which pointed out as rocking has little effects on the peak bearing deformation or axial forces and, however, emphasize the needs for considering it in designing the isolation system of this type of structures.

ACKNOWLEDGEMENTS

This work has been partially supported by MIUR (Ministry of Education, University and Research) under the project "Dynamic response of linear and nonlinear structures: modelling, testing and identification" (PRIN 2009).

REFERENCES

Abe M., Yoshida J., Fujino Y. (2004), ”Multiaxial Behaviors of Laminated Rubber Bearings and Their Modeling. II: Modeling”, ASCE Journal of Structural Engineering, **130**:1133-1144.

Abrahamson, N.A., Schneider, J.F. and Stepp, J.C. (1991). Empirical Spatial Choerency Functions for Application to Soil–Structure Interaction Analyses. *Earthquake Spectra*. **7**:1-27.

Carelli, M.D., et al. (2004), “The design and safety features of the IRIS reactor”, *Nuclear Engineering and Design*, **230**: 151–167.

Castellani, A., Stupazzini, M. and Guidotti, R. (2012). Free- fi eld rotations during earthquakes: Relevance on buildings. *Earthquake Engineering and Structural Dynamics*. **41:**875 – 891, doi: 10.1002/eqe.1163.

Clough, R.W. and Penzien, J. (1975). Dynamics of structures. McGraw-Hill, New York, NY.

De Grandis, S., Domaneschi, M., Perotti, F. (2009). A numerical procedure for computing the fragility of NPP components under random seismic excitation. *Nuclear Engineering and Design*. **239**:2491-2499.

EN 1998-1 (2005). Eurocode 8. Design of structures for earthquake resistance. Part 1: General rules, seismic actions and rules for buildings.

ENEA Centro Ricerche Bologna, Report XFIP-LP2-001 (2010).

Forni M., Poggianti A., Bianchi F., Forasassi G., Lo Frano R., Pugliese G., Perotti F., Corradi dell’Acqua L., Domaneschi M., Carelli M.D., Ahmed M.A., Maioli A. (2009). Seismic Isolation of the IRIS Nuclear Plant. *ASME Pressure Vessels and Piping Conference (PVP 2009)*, Prague; Code 80491. (2010) *American Society of Mechanical Engineers, Pressure Vessels and Piping Division (Publication) PVP*. **8**:289-296. ISSN: 0277027X. ISBN: 978-079184371-0.

Luco, J.E. and Wong, H.L. (1986). Response of a rigid foundation to a spatially random ground motion. *Earthquake Engineering and Structural Dynamics*.**14:**891–908.

Martinelli, L., Barbella, G. and Feriani, A. (2011). A numerical procedure for simulating the multi-support seismic response of submerged floating tunnels anchored by cables. *Engineering Structures*. **33:**2850–2860. doi:10.1016/j.engstruct.2011.06.009.

Monti, G., Nuti, C. and Pinto, P.E. (1996). Nonlinear response of bridges under multisupport excitation. *Journal of Structural Engineering*.**112**:1147–1159.

Perotti, F., Domaneschi, M., Corradi, L., Mantegazza, D.C., Bianchi, G. (2011). The seismic fragility of base-isolated NPP buildings. *Proc. of*, SMiRT 21, *Paper ID 205*, 6-11 November, New Delhi, India.

Politopoulos, I. (2009). Response of seismically isolated structures to rocking type excitations. *Earthquake Engineering & Structural Dynamics*. **39**: 325-342.

Rivin, E.I. (2003). Passive vibration isolation, The America Society of Mechanical Engineers, New York , NY. ISBN: 0-7918-0187-X.

Ryan, K.L. and Chopra, A.K. (2006). Estimating Seismic Demands for Isolation Bearings with Building Overturning Effects. *Journal of Strucural Engineering*. **132**:**7**, 1118-1128**,** doi:10.1061/(ASCE)0733-9445(2006).

Shinozuka, M. (1972). Monte Carlo solution of structural dynamics. *Computer and Structures*. **2**:855–874.